Water Science & Technology

Water Science & Technology Vol 87 No 1, 304 doi: 10.2166/wst.2022.431

Enhanced catalytic activity and stability of composite of cellulose film and nano zero-valent iron on *Juncus effusus* for activating peroxydisulfate to degrade Rhodamine B dye

Shengli Zhang *, Menglin Li, Yuhang Xu, Sisi Qin, Haibo Hu, Hongwei Yang and Kai Su

Faculty of Geosciences and Environmental Engineering, Southwest Jiaotong University, Chengdu 611756, Sichuan, China
*Corresponding author. E-mail: zhang222@home.swjtu.edu.cn

SZ, 0000-0001-8977-0228

ABSTRACT

In this study, a novel peroxydisulfate (PDS) activator (CF-nZVI-JE) was prepared via in-situ loading nano zero-valent iron (nZVI) on *Juncus effusus* (JE) followed with wrapping a layer of cellulose film (CF). The CF-nZVI-JE had the same 3D structure as the JE, being easy to separate from aqueous solution. The loaded nZVI existed single nanoparticles with a size of 60–100 nm except chain-type agglomeration of nanoparticles due to the stabilization of JE fibers. The activation performance of the CF-nZVI-JE for PDS was evaluated with Rhodamine B (Rh B) as a representative pollutant. Under the optimal activating conditions, the degradation rate of Rh B reached 99% within 30 min in the CF-nZVI-JE/PDS system. After five cycles, the degradation rate of Rh B was still over 85%, suggesting that the CF-nZVI-JE had good reusability. More interestingly, $SO_4^{\cdot-}$ and ·OH radicals were simultaneously detected in the CF-nZVI-JE/PDS system, but only $SO_4^{\cdot-}$ existed in the JE-ZVI/PDS system, suggesting the different activation mechanism. Meanwhile, the introduction of CF not only facilitated to the mineralization of Rh B but also significantly reduced the release amount of iron ions. Hence, the CF-nZVI-JE can be employed as a promising PDS activator for the treatment of organic wastewater.

Key words: *Juncus effusus*, nano zero-valent iron, persulfate, Rhodamine B

HIGHLIGHTS

- The prepared CF-nZVI-JE had the same 3D structure as JE, which can stabilize nZVI.
- nZVI existed as single nanoparticles and chain-type agglomeration of nanoparticles.
- Rh B degradation was involved in $SO_4^{\cdot-}$ and HO· in the CF-nZVI-JE/PDS system.
- CF-nZVI-JE facilitated the mineralization of Rh B compared with the nZVI-JE.
- CF prevented the leakage of nZVI and reduced the release amount of iron ions.

GRAPHICAL ABSTRACT

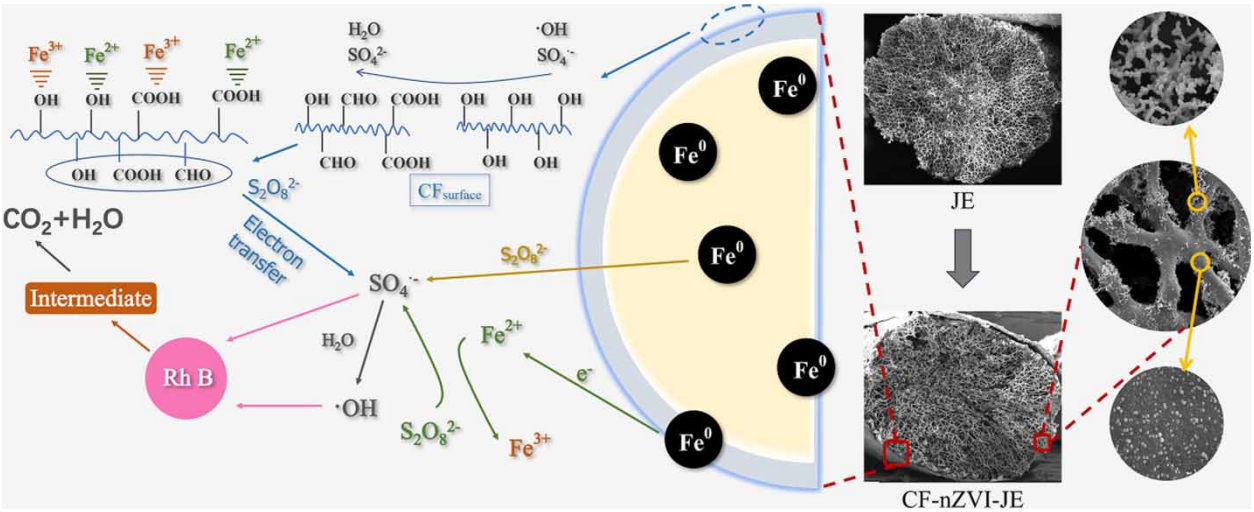

INTRODUCTION

With the rapid development of industrialization, emissions of organic wastewater are on the rise, causing serious harm to the ecological environment and human health (Lee *et al.* 2020; Ledakowicz & Pazdzior 2021). As one of the main organic waste waters, dye wastewater has the characteristics of large chromaticity, high content, stable structure, and large change in pH (Matzek & Carter 2016; Collivignarelli *et al.* 2019). At present, various methods such as microbial degradation (Hameed & Ismail 2021), photodegradation (Zheng *et al.* 2006), adsorption (Zhang *et al.* 2021), chemical precipitation (Mateus *et al.* 2020), membrane process (Nawaz *et al.* 2021) and advanced oxidation method (Elmobarak *et al.* 2021), have been applied in the degradation of dye wastewater. Among them, advanced oxidation processes (AOPs) have currently become a research hotspot because they can effectively degrade macromolecular organic pollutants into small molecules and finally achieve their mineralization (Ma *et al.* 2021; Khajouei *et al.* 2022).

In the reported AOPs (e.g., ozonation, UV irradiation, photocatalysis, Fenton reaction, persulfate, etc), persulfate can generate sulfate radical ($SO_4^{\cdot-}$), which has high redox potential, a longer half-life and wider pH range compared with •OH based on Fenton system (Yin *et al.* 2018; Gao *et al.* 2020). Peroxydisulfate (PDS) and peroxymonosulfate (PMS) are widely used as $SO_4^{\cdot-}$ precursors. At present, the common methods for activating persulfate mainly include UV light (Lau *et al.* 2007), heating (Waldemer *et al.* 2007), ultrasound (Kyzas *et al.* 2022), transition metals and their oxides (Anipsitakis & Dionysiou 2004), etc.

Because of the wide source, low price and environmental friendliness, iron-based materials have been widely used to activate persulfate for removing organic pollutants in wastewater (Dong *et al.* 2017; Guo *et al.* 2020). Especially, nZVI exhibits higher reactive due to the high specific surface area and small size, which could effectively activate persulfate to degrade organic pollutants (Fu *et al.* 2014; Chokejaroenrat *et al.* 2015). However, nZVI has the problems of easy agglomeration, easy oxidation, poor stability and difficult separation from the solution after use, which limits its application (Xiao *et al.* 2020; Wang *et al.* 2021). To solve the above problems, some researchers loaded nZVI onto the solid materials like carbon (Li *et al.* 2022), bentonite (Baldermann *et al.* 2021), kaolinite (Lakkaboyana *et al.* 2021) and zeolite (Eljamal *et al.* 2021) for removing pollutants more effectively. However, most of the reported materials are powder, which are still difficult to recover after use. By contrast, the macro-materials possessing a three-dimensional (3D) structure not only are easy to separate from aqueous solution but also can expose more active sites (Tan *et al.* 2021).

Juncus effusus, a perennial herbaceous fiber, has been cultivated extensively in many places in China (Wang *et al.* 2009). It has a natural 3D structure and high specific surface area, being a good carrier for nZVI (Zhou *et al.* 2020). Nevertheless, JE fiber has strong hydrophobicity, which brings some obstacles to the introduction of active groups. According to the recent research from our group, the ethanol/aqueous solution can help to overcome the hydrophobicity of JE without destroying its 3D structure (Zhang *et al.* 2022). But to the best of our knowledge, there is no report on loading nZVI on the JE.

Herein, an efficient PDS activator CF-nZVI-JE was facilitated by in-situ loading nZVI on the 3D structure of JE followed with wrapping a layer of cellulose film outside as displayed in Figure 1. The physical morphology and chemical compositions of the CF-nZVI-JE were characterized by SEM, XRD and FTIR. The activation performance for PDS was evaluated by using Rhodamine B (Rh B) as a representative pollutant. The effect of coexistence anions including Cl^-, NO_3^- and SO_4^{2-} on Rh B degradation and the reusability of CF-nZVI-JE were investigated. Meanwhile, the degradation mechanism of Rh B in the CF-nZVI-JE/PDS system was explored. The CF-nZVI-JE can not only stabilize nZVI and prevent its leakage, but also facilitate the mineralization of Rh B and reduce the release amount of iron ions. Hence, it can be employed as a promising PDS activator for the treatment of organic wastewater.

EXPERIMENTAL MATERIALS AND METHODS

Materials

Sodium borohydride ($NaBH_4$), ferrous sulfate ($FeSO_4{\cdot}7H_2O$), Rhodamine B (Rh B), potassium peroxydisulfate ($K_2S_2O_8$), sodium chloride (NaCl), sodium sulfate (Na_2SO_4), sodium sulfate ($NaNO_3$), t-butyl alcohol (TBA, $C_4H_{10}O$), methanol, ethanol and dimethylsulfoxide (DMSO) were purchased from Chengdu Kelong Chemical Co., Ltd, which were analytical grade and used without any purification. Nitrogen was purchased from Chengdu Shimao Gas Co., Ltd JE was purchased from Guangxi Jintu Ecological Agriculture Co., Ltd Cotton pulp cellulose was provided by Bailu Chemical Fiber Group Ltd, China. Aqueous solution of tetrabutylammonium hydroxide (TBAH, 40 wt%) was obtained from Shanghai Meryer Chemical Technology Co. Ltd, China.

Synthesis of the CF-nZVI-JE

First, JE was treated in 50% ethanol/aqueous solution for 10 min, and then immersed in a certain concentration of $FeSO_4$ solution for 30 min under N_2 gas protection. Afterwards, the immersed JE was transferred onto polyethylene webs (Figure S1), and 8 g/L of $NaBH_4$ solution was dropwise added until no obvious bubbles appeared. The obtained sample was denoted as nZVI-JE. Next, the nZVI-JE was put in a 2% cellulose solution followed with regeneration and washing by deionized water with dissolved O_2 excluded. The resultant sample was denoted as CF-nZVI-JE.

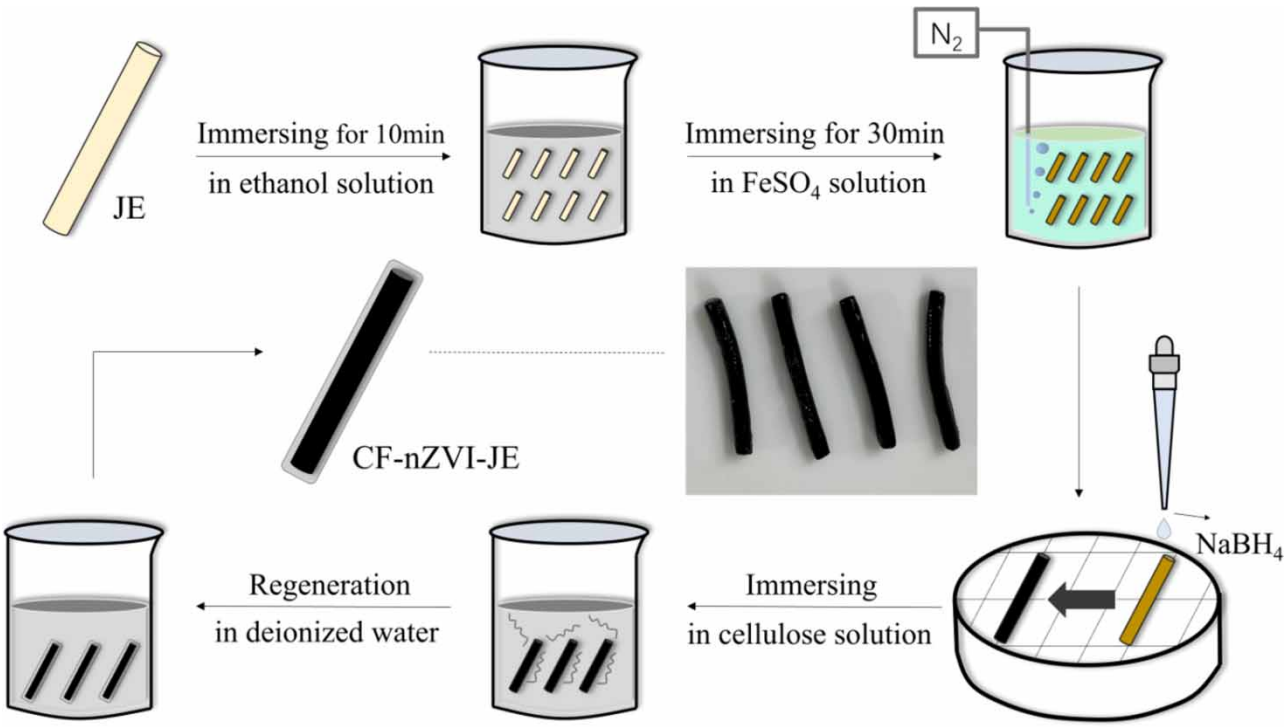

Figure 1 | Synthetic scheme for the preparation of CF-nZVI-JE.

Degradation experiments of Rh B

The activation performance of the CF-nZVI-JE for PDS was evaluated with Rh B as a representative pollutant. The stock solution of Rh B (1,000 mg/L) was firstly prepared and further diluted to the needed concentrations. The batch experiments were done in a series of 250 mL erlenmeyer flask filled with 100 mL of Rh B solution. After adding a PDS solution with a certain concentration, a preset amount of CF-nZVI-JE was put into. The reaction was done for different time at 25 °C in a constant temperature oscillation box. The initial solution pH (2.0–10.0) was adjusted by 1 mol/L NaOH and 1 mol/L HCl. At a fixed reaction interval, 0.4 mL reaction solution was taken out with immediately adding the same volume of methanol to terminate the reaction. Afterwards, the Rh B concentration in the solution was measured using a UV-VIS spectrophotometer at a wavelength of 554 nm. The degradation rate η and degradation amount q of Rh B was calculated by Equations (1) and (2), respectively.

$$\eta = \frac{C_0 - C_e}{C_0} \times 100\% \tag{1}$$

$$q = \frac{(C_0 - C_t) \times V}{m} \tag{2}$$

C_0 (mg/L) and C_e (mg/L) are the initial concentration and equilibrium concentration of Rh B, m (g) is the dosage of the activator, and V (L) is the volume of the solution. All experiments were conducted in triplicate.

The influence of different anions including Cl^-, NO_3^- and SO_4^{2-} on Rh B degradation was investigated by fixing Rh B concentration at 50 mg/L. Their concentrations were 200 mg/L, respectively.

Cycle experiment was performed as follows: take out the CF-nZVI-JE from the first reaction system at 20 min, and then add it to the second reaction system. After that, further add to the next reaction system (Figure S2).

Characterizations

The physical morphologies of the JE and CF-nZVI-JE were observed on a Apreo 2C scanning electron microscope (Thermo Scientific., Holland) equipped with X-ray energy dispersive spectroscopy (OXFORD ULTIM Max65). To improve the conductivity of the samples and the quality of the SEM images, a layer of gold film was coated on the surface of the samples. The crystal structure of the JE and CF-nZVI-JE was analyzed by a D8 Advanced X-ray diffractometer (Bruker, Germany) using Cu-Kα radiation. The surface functional groups of the JE and CF-nZVI-JE were measured by a FTIR spectroscope (Nicolet iS50, Thermo Fisher Scientific, America) with an ATR accessory. The data in the range of 4,000–400 cm^{-1} were recorded at a resolution of 4 cm^{-1}.

RESULTS AND DISCUSSION

Characterization of the samples

The SEM images of the cross-section of the JE and CF-nZVI-JE are shown in Figure 2. From Figure 2(a) and 2(b), it can be seen that JE had a natural 3D network structure, and the surface of JE fiber was relatively smooth. After in-situ loading nZVI, the 3D structure of JE was still clearly visible for the CF-nZVI-JE (Figure 2(d)). Some chain-type agglomeration of nanoparticles appeared on JE fibers and between the gaps (Figure 2(f)). More interestingly, a large number of nanoparticles with a size of 60–100 nm were found to be uniformly dispersed on the surface of JE fibers (Figure 2(g)). According to the element distribution of Fe, they were confirmed to be made from element Fe (Figure 2(e)). The formation of the dispersed nZVI could be attributed that Fe^{2+} ions were firstly immobilized the by -OH groups on JE cellulose, and then were in-situ reduced to nZVI. They not only had a high specific surface area but also provided more active sites for the subsequent reactions. Meanwhile, it was evident that a layer of cellulose film with a thickness of about 20 μm wrapped the whole nZVI-JE (Figure 2(c)), which can not only be separated easily from aqueous solution but also prevent the leakage of nZVI.

Figure S3 showed the XRD patterns of the JE and CF-nZVI-JE. Compared with the XRD pattern of JE, the characteristic diffraction peak of Fe^0 can be observed at 45.84 ° on the XRD pattern of the CF-nZVI-JE. Furthermore, it was weak and broad, verifying that the Fe^0 particles loaded on the JE had a small grain size.

Figure S4 displayed the FTIR spectra of the JE and CF-nZVI-JE. Compared with the spectrum of JE, the adsorption peaks at 3,340, 1,245 and 1,030 cm^{-1} related to the O-H stretching and bending vibrations gave a decrease after Fe^0 was loaded. The reason was due to the formed hydrogen bond between -OH and Fe nanoparticles (He *et al.* 2007). The band at 1,725 cm^{-1}

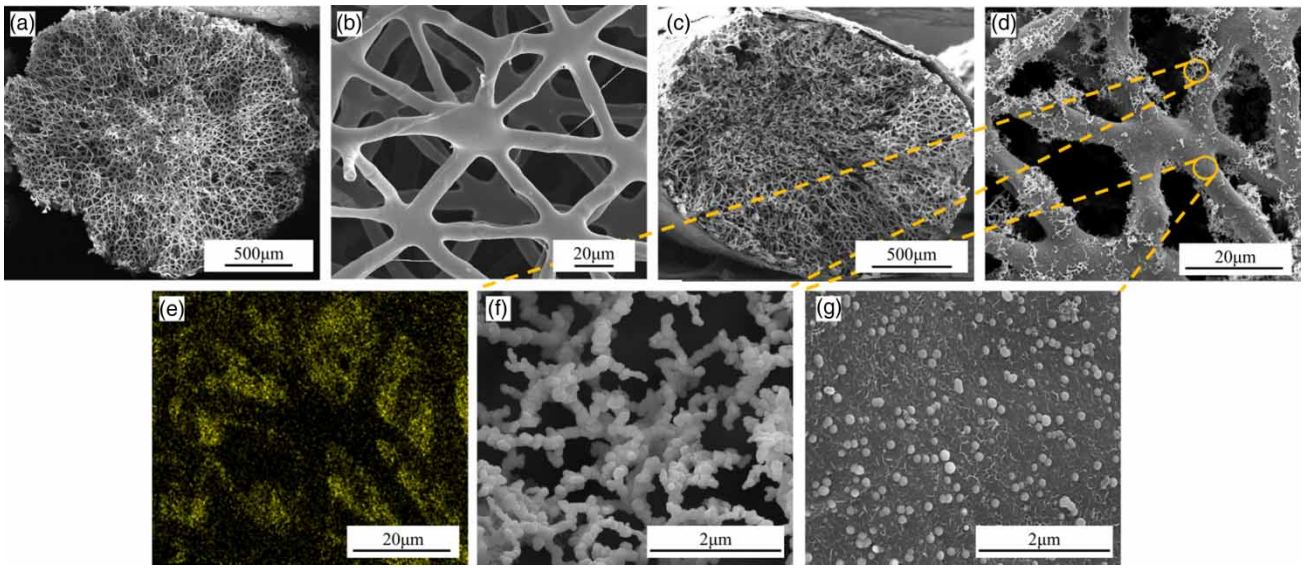

Figure 2 | SEM images of the cross-section of the JE (a, b) and CF-nZVI-JE (c-f), and X-ray mapping of element Fe in the CF-nZVI-JE (g).

assigned to the C = O group displayed a red shift because Fe formed strongly-bound inner-sphere complex (-COOFe) with the carboxyl group (Dong *et al.* 2016). At the same time, the strong adsorption was observed between 400 and 500 nm due to the stretching vibrations of Fe-O (Zhang *et al.* 2019). As far as the peaks at 1,600 and 1,510 cm^{-1} originating from aromatic ring C = C stretching of lignin disappeared, it was because of the dissolution of lignin in the alkali solution.

Rh B degradation in different systems

The effects of different reaction systems including PDS, JE/PDS, CF/PDS, CF-JE/PDS and CF-nZVI-JE/PDS on Rh B degradation were investigated, and the results were displayed in Figure 3(a). It can be seen that the degradation rates of Rh B were 20 and 22% at 60 min in the PDS and JE/PDS systems, respectively. This indicated that the degradation abilities of PDS and JE/PDS for Rh B were limited. In the CF/PDS and CF-JE/PDS systems, the degradation rates of Rh B were slightly improved to 30 and 32% at 60 min, suggesting that the CF had a positive effect on Rh B degradation. By contrast, a sharp increase was observed for the degradation rate of Rh B in the CF-nZVI-JE/PDS system, demonstrating that CF-nZVI-JE can effectively activate PDS to produce free radicals for degrading Rh B. Moreover, nZVI played a key role in the activation of PDS.

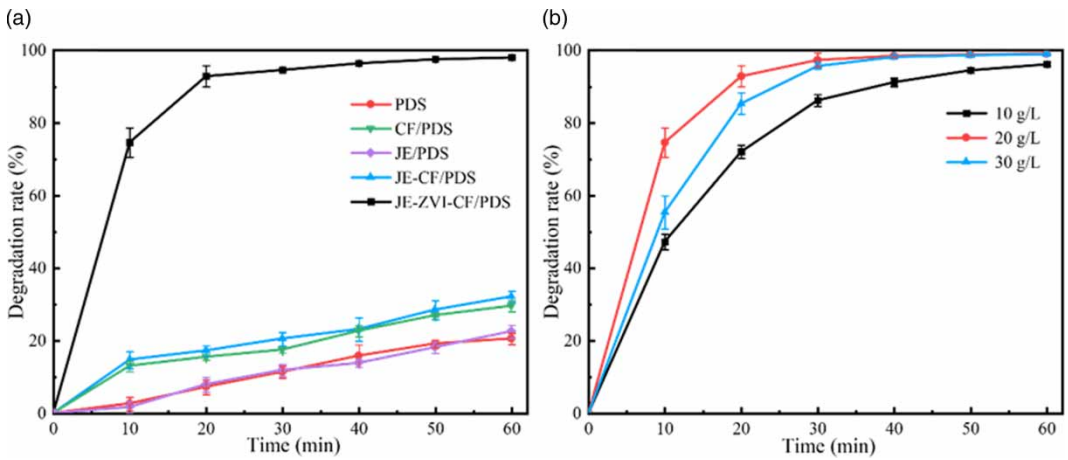

Figure 3 | Rh B degradation in different systems (a) and the effect of Fe^{2+} concentration used at the preparation stage of the CF-nZVI-JE on Rh B degradation (b) ([Rh B] = 50 mg/L, $[K_2S_2O_8]$ = 1 g/L, JE = 0.5 g/L, pH = 4).

Effect of Fe^{2+} concentration on Rh B degradation

Fe^{2+} concentration in the preparation of the CF-nZVI-JE directly influenced the nZVI amount loaded on the JE, which further affected the degradation rate of Rh B. Hence, the effect of Fe^{2+} concentration at the immersing stage on Rh B degradation was investigated. From the results shown in Figure 3(b), it can be seen that the degradation rate of Rh B firstly increased and then decreased with increasing Fe^{2+} concentration from 10 to 30 g/L. At 20 min, the degradation rates were 72, 92 and 85%, respectively. The reason was that the lower Fe^{2+} concentration was, the less the generated nZVI, which led to insufficient $SO_4^{\cdot-}$ to participate in the reaction (Wang *et al.* 2018). However, too high Fe^{2+} concentration would generate too much nZVI. As a result, it could consume $SO_4^{\cdot-}$, reducing the degradation rate of Rh B (Fu *et al.* 2020). Hence, 30 g/L of Fe^{2+} concentration was used in subsequent experiments.

Effects of activation conditions on Rh B degradation

In view that solution pH played an important role in the degradation reaction, the effect of initial pH on Rh B degradation was investigated in the CF-nZVI-JE/PDS system. From the results presented in Figure 4(a), it was evident that the reaction

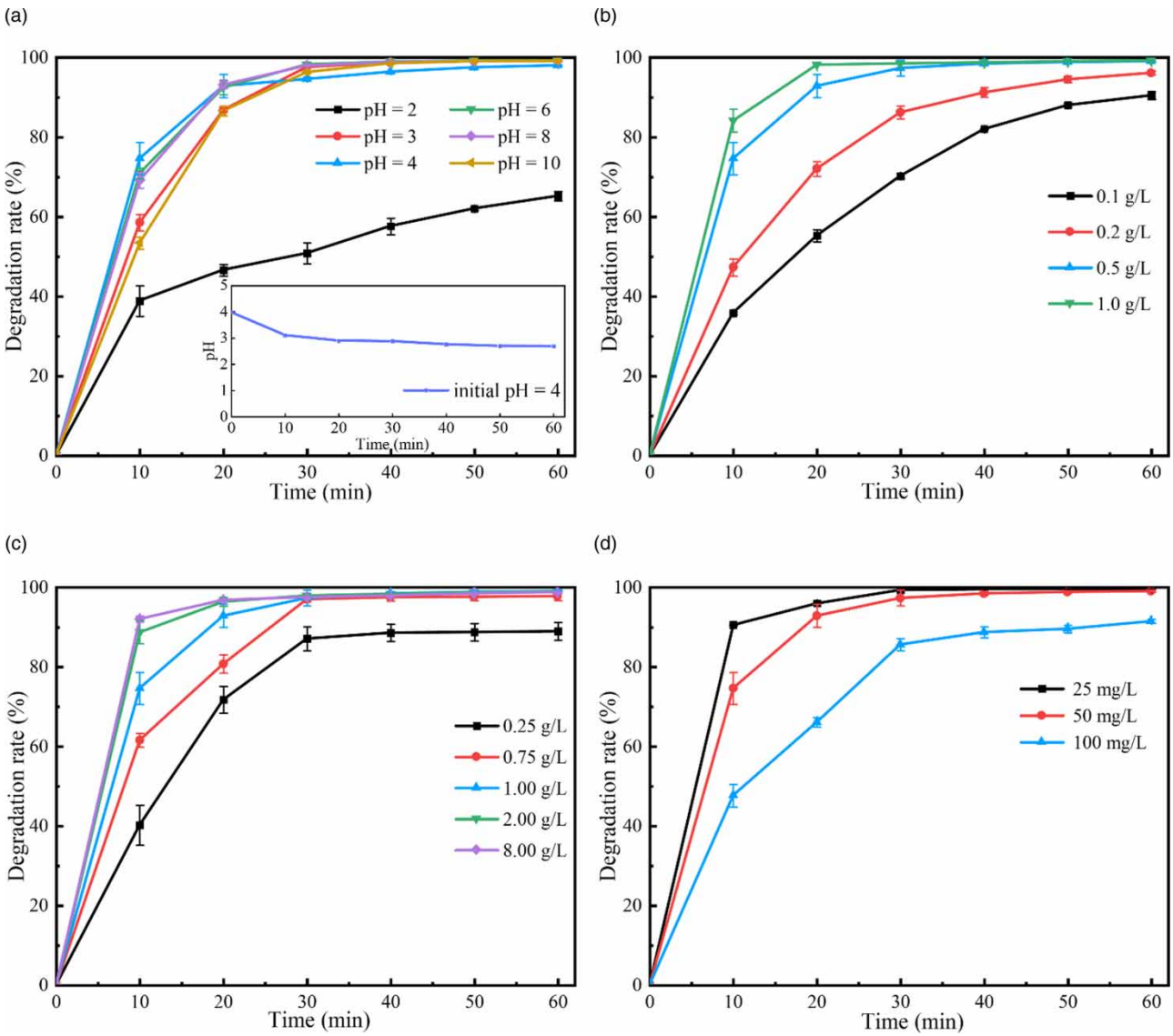

Figure 4 | Effects of initial pH value (a), CF-nZVI-JE dosage (b), PDS concentration (c) and initial Rh B concentration (d) on the degradation rate of Rh B at different reaction time.

system had a good degradation performance and the degradation rate of Rh B reached 98% within 30 min in the pH range from 3 to 10. This phenomenon was attributed that the released Fe^{2+} and H^+ in the acidic environment stimulated the production of $SO_4^{\cdot-}$. By contrast, more ·OH radicals were formed in the alkaline environment at the beginning of the reaction. However, its oxidation activity was weaker than $SO_4^{\cdot-}$, causing to lower the degradation rate of Rh B at the initial stage. This result was similar to the previous report (Jiang *et al.* 2018). When initial solution pH was decreased to 2, the degradation rate of Rh B decreased significantly from 98% to 50% at 30 min. It was because too much $SO_4^{\cdot-}$ became a self-consuming agent, negatively affecting the reaction (Hou *et al.* 2011; Zhang *et al.* 2018). Meanwhile, the final pH of the solution was also investigated for the system without adjusting the initial pH. It can be seen that the final pH rapidly decreased from 4 to 3 within 10 min, and then gave a slow decrease with delaying the reaction time.

The effect of CF-nZVI-JE dosage on Rh B degradation was shown in Figure 4(b). With the increasing of the CF-nZVI-JE dosage, the degradation rate of Rh B increased. It was due to the fact that more CF-nZVI-JE provided more nZVI which can activate PDS to produce more free radicals in the reaction system.

When other activation conditions were fixed, the effect of PDS concentration on Rh B degradation is shown in Figure 4(c). It was evident that the degradation rate of Rh B showed a gradual increase with increasing PDS concentration. For instance, when PDS concentrations were 1, 2 and 8 g/L, the degradation rates of Rh B were 74, 89 and 92% at 10 min, respectively. The reason was that increasing PDS concentration can provide more $SO_4^{\cdot-}$ in the presence of CF-nZVI-JE, facilitating the Rh B degradation. Of course, excess PDS could become the scavenger of $SO_4^{\cdot-}$ produced by itself (Yang *et al.* 2011; Wang *et al.* 2017).

Figure 4(d) shows the effect of initial Rh B concentration on the degradation. As the initial concentration increased from 25 to 100 mg/L, the degradation rates of Rh B were decreased from 90% to 47% at 10 min. Further delaying reaction time to 60 min, 99% Rh B was degraded for the initial concentration of 25 and 50 mg/L, while 90% for 100 mg/L. It was because fixing PDS concentration and CF-nZVI-JE dosage, the amount of the produced free radicals was certain (Barzegar *et al.* 2018). Thus, the higher concentration of Rh B was not entirely degraded by the limited free radicals (Zhang *et al.* 2009).

Effect of coexisting anions on Rh B degradation

The presence of inorganic ions was common in real water environment. Hence, the effect of three typical anions including NO_3^-, Cl^- and SO_4^{2-} on Rh B degradation was investigated in the CF-nZVI-JE/PDS system. From the results as presented in Figure 5(a), NO_3^- and SO_4^{2-} displayed a slight negative effect on Rh B degradation compared with Cl^-. The reason was that nZVI was more vulnerable to corrosion in the presence of Cl^- (Qiong 2020). The faster the corrosion of nZVI was, the more the generated Fe^{2+}. As a result, excessive Fe^{2+} would remove the free radicals such as $SO_4^{\cdot-}$ and ·HO, reducing the

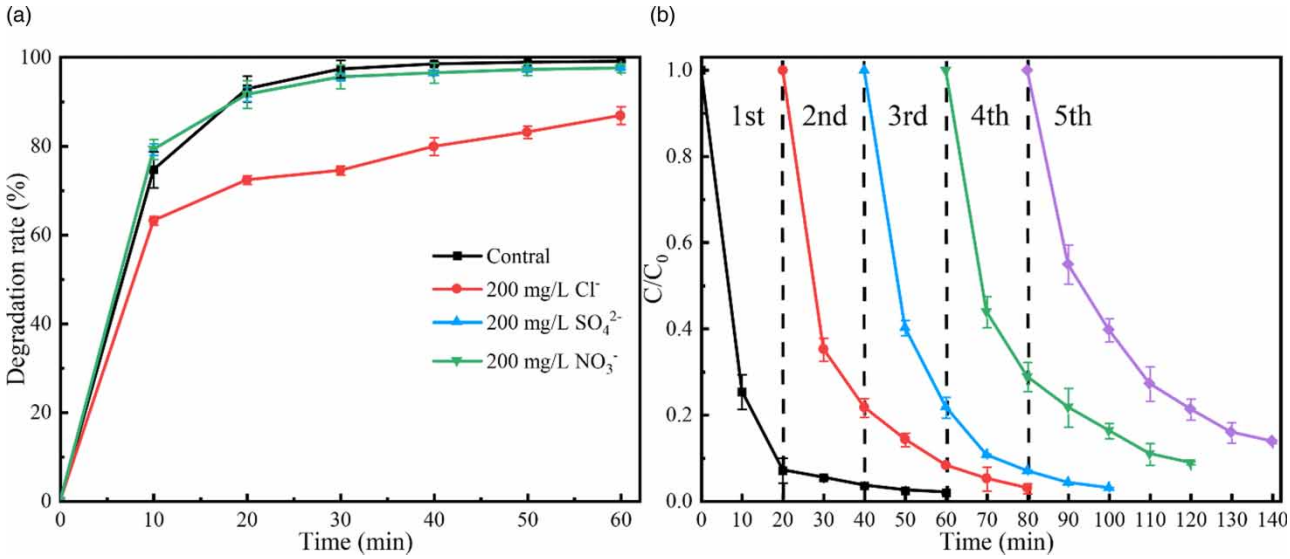

Figure 5 | Effect of coexisting anions including NO_3^-, Cl^- and SO_4^{2-} on Rh B degradation (a) and the recycling performance of the CF-nZVI-JE (b) (T = 25 °C, [Rh B] = 50 mg/L, [$K_2S_2O_8$] = 1 g/L, JE = 0.5 g/L, pH = 4).

degradation rate of Rh B (Equation (3)). In addition, Cl^- would react with $SO_4^{\cdot-}$ and ·HO to reduce free radicals in the system (Equation (4)).

$$Fe^{2+} + SO_4^{\cdot-}/HO\cdot \rightarrow Fe^{3+} + SO_4^{2-} + OH^- \quad (3)$$

$$Cl^- + SO_4^{\cdot-}/HO\cdot \rightarrow Cl\cdot + SO_4^{2-} \quad (4)$$

Recycling performance of the CF-nZVI-JE

The recycling performance of persulfate activator is very important for its application, so that of the CF-nZVI-JE was investigated as presented in Figure 5(b). It was clear that the degradation rate of Rh B reached 98, 97, 96, 91 and 86% from the first to fifth cycles at 60 min, respectively, suggesting that the CF-nZVI-JE had good reusability. Nevertheless, a small difference can be observed at the initial stage. At 10 min, the degradation rate of Rh B was 75, 65, 60, 56 and 43%, respectively. It could be related to the reduce of the active sites on the JE-ZVI-CF due to the dissolution of Fe^0.

Reaction kinetics

To study the reaction rate of Rh B degradation in the CF-nZVI-JE/PDS system, pseudo-first-order (Equation (5)) and pseudo-second-order (Equation (6)) kinetic models were used to analyze the kinetic data.

$$\ln(q_e - q_t) = \ln q_e - k_1 t \quad (5)$$

$$\frac{t}{q_t} = \frac{1}{k_2 q_e^2} + \frac{t}{q_e} \quad (6)$$

q_e and q_t (both in mg/g) are the degradation amount of the Rh B at equilibrium and time t, k_1 is the rate constant of the pseudo-first-order kinetic equation (min^{-1}), and t is the reaction time (min), k_2 is the rate constant (g/mg · min) of the pseudo-second-order kinetic equation.

The fitting curves and related parameters were shown in Figure S5 and Table 1, respectively. It was obvious that the correlation coefficient R^2 obtained by the pseudo-second-order kinetic model was higher than that of the pseudo-first-order kinetic model. Moreover, the $q_{e,cal}$ values were also closer to the experimental values ($q_{e,exp}$). Hence, Rh B degradation in the CF-nZVI-JE/PDS system fitted the pseudo-second-order kinetic model, suggesting that the degradation process was involved in chemical adsorption. A similar result has been reported in previous literature (Chen *et al.* 2021). Meanwhile, the values of k_2 gave a decrease with increasing the initial concentration of Rh B, suggesting that the degradation of higher concentration of Rh B needed longer time.

DEGRADATION MECHANISM

Ethanol can react with $SO_4^{\cdot-}$ and ·OH rapidly, while the reaction rate constant of t-butyl alcohol with ·OH is much greater than $SO_4^{\cdot-}$. Therefore, the combination of ethanol and t-butyl alcohol is commonly used to detect $SO_4^{\cdot-}$ and ·OH free radicals. In the present study, the free radicals that were mainly responsible for Rh B degradation in the CF-nZVI-JE/PDS system were determined via adding excessive free radical quenchers ethanol and t-butyl alcohol.

From the results shown in Figure 6(a), it can be seen that about 99% of Rh B was degraded at 30 min without a quencher. When ethanol and tertbutyl alcohol were added to the system, the degradation rates of Rh B were 55 and 92% at 30 min, respectively. This indicated that both $SO_4^{\cdot-}$ and ·OH were involved in the degradation of Rh B in the CF-nZVI-JE/PDS

Table 1 | Parameters of kinetic models for Rh B degradation by the CF-nZVI-JE/PDS

		Pseudo-first-order			Pseudo-second-order		
C_0(mg/L)	$q_{e,\ exp}$ (mg/g)	k_1 (min^{-1})	q_e (mg/g)	R^2	k_2 (g/(mg·min))	q_e (mg/g)	R^2
25	4.96	0.066	1.85	0.7622	0.218	5.04	0.9990
50	9.41	0.068	4.15	0.8888	0.102	9.48	0.9990
100	17.02	0.058	12.59	0.9403	0.019	17.33	0.9921

system, and $SO_4^{\cdot-}$ was the main free radical. In comparison, the degradation of Rh B was only involved in $SO_4^{\cdot-}$ in the JE-ZVI/PDS system, and ·OH contributed relatively insignificant (Figure 6(b)). Therefore, the activation mechanism of the CF-nZVI-JE for PDS could include three ways: (1) redox action of Fe^{2+}/Fe^{3+}; (2) nZVI mediated activation; (3) O-containing groups as an activator of the electron-transfer mediator. There were a large number of –OH groups on the CF, which can be oxidized to –CHO/COOH groups and the following reactions (Equations (7) and (8)) took place (Pu *et al.* 2014; Yan *et al.* 2015). The produced free radicals can effectively destroy the structure of Rh B, and the formed intermediates were further mineralized into CO_2 and H_2O.

$$CF_{surface} - OH + S_2O_8^{2-} \rightarrow CF_{surface} - O\cdot + SO_4^{\cdot-} + HSO_4^- \quad (7)$$

$$CF_{surface} - OOH + S_2O_8^{2-} \rightarrow CF_{surface} - OO\cdot + SO_4^{\cdot-} + HSO_4^- \quad (8)$$

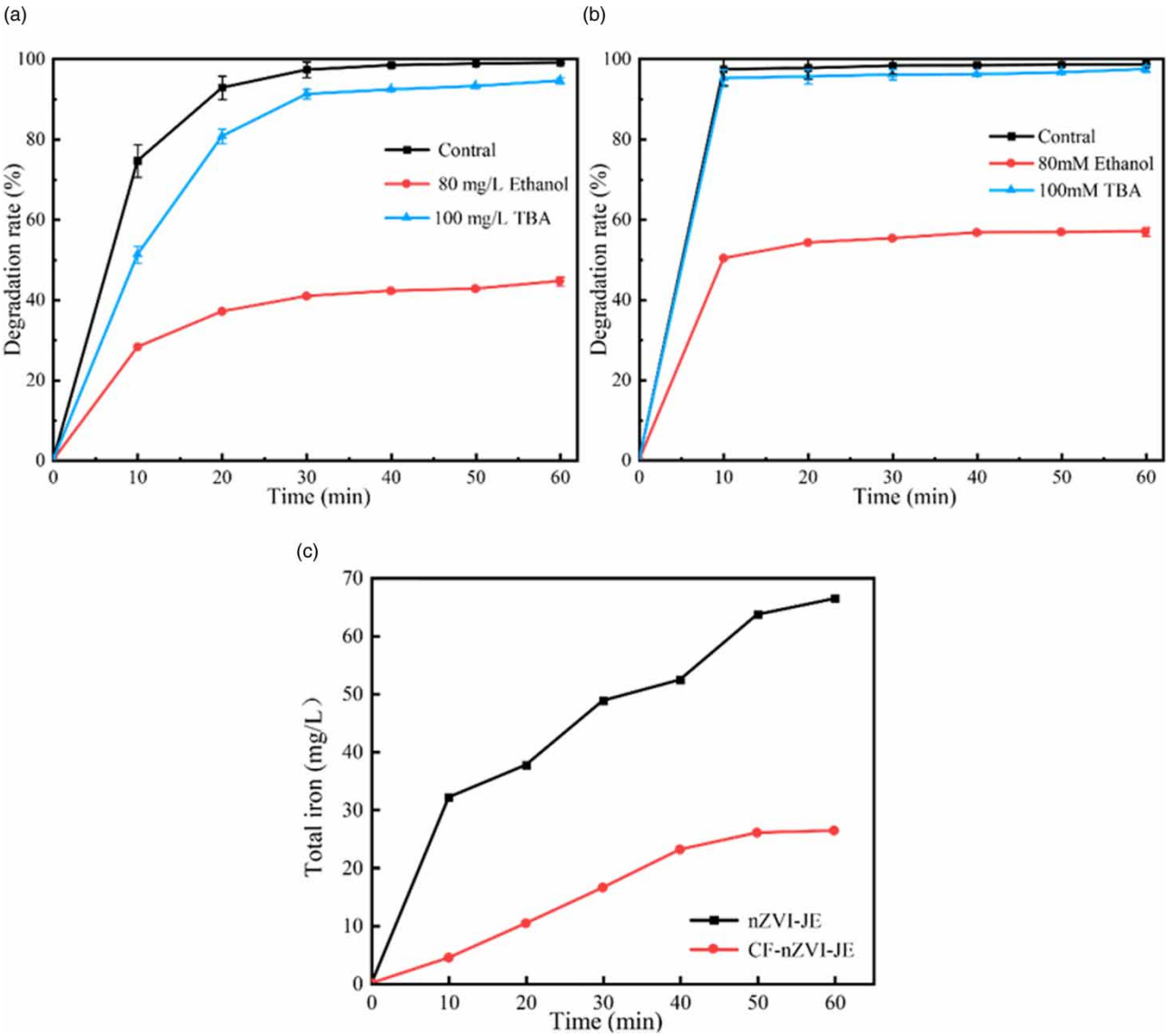

Figure 6 | Effects of different radical scavengers on Rh B degradation in the CF-nZVI-JE/PDS (a) and nZVI-JE/PDS (b) systems, and the release amount of iron ions in the CF-nZVI-JE/PDS and nZVI-JE/PDS systems (c).

In additon, compared with the nZVI-JE/PDS system, the release amount of iron ions gave an obvious decrease in the CF-nZVI-JE/PDS system as shown in Figure 6(c). The phenomenon could be related to the following two aspects: One was that the existence of the CF reduced the dissolution of Fe^0, the other was that the O-containing functional groups like –COOH and –OH on the CF fixed part of the released iron ions.

The UV-Vis absorption spectra of the solution during the Rh B degradation by the nZVI-JE/PDS and CF-nZVI-JE/PDS are shown in Figure 7. It can be seen that although the JE-ZVI/PDS can quickly destroy the chromogenic functional groups of Rh B at 554 nm, the formed intermediate products did not change significantly with delaying reaction time (Dai *et al.* 2022). In contrast, the decolorization of Rh B in the CF-nZVI-JE/PDS system was slow at the beginning of the reaction, but the intermediates produced in the system gave an obvious decrease with the reaction time increasing. This suggested that the introduction of CF was conducive to the mineralization of Rh B (Gao *et al.* 2016).

To visually exhibit the degradation process of Rh B in the CF-nZVI-JE/PDS and nZVI-JE/PDS systems, the solution at different reaction time was irradiated under 365 UV light and the results are shown in the inset of Figure 7. It was evident that the decolorization of Rh B was quickly completed within 10 min in the JE-ZVI/PDS system, but since then the solution emitted a green fluorescence at 492 nm. By contrast, in the CF-nZVI-JE/PDS system, fluorescence color of the solution changed from red to orange and to green during the initial 30 min. Afterward, the green fluorescence became weak with delaying the reaction time, suggesting the gradual degradation of the formed intermediate products (Wu *et al.* 2020). This was consistent with the UV-Vis result that Rh B was degraded into some intermediate products firstly and then the intermediate products were further mineralized in the CF-nZVI-JE/PDS system.

According to the above results and analysis, the degradation mechanism of Rh B in the CF-nZVI-JE/PDS system is proposed in Figure 8. Firstly, $SO_4^{\cdot-}$ and ·OH free radicals were produced by the redox action of Fe^{2+}/Fe^{3+}, nZVI mediated activation and O-containing groups as an activator of the electron-transfer mediator. Then, the chromogenic functional groups of Rh B at 554 nm were destroyed by the formed free radicals, and the intermediate products were further mineralized. Meanwhile, due to the existence of CF, the dissolution of Fe^0 was reduced, and the O-containing functional groups like –COOH and –OH on the CF fixed part of the released iron ions.

CONCLUSIONS

In this study, a new PDS activator CF-nZVI-JE was facilitated, which possessed the same 3D structure as JE. Due to the stabilization from the JE, the nZVI in-situ loaded on the JE existed in two forms: single nanoparticles with a size of

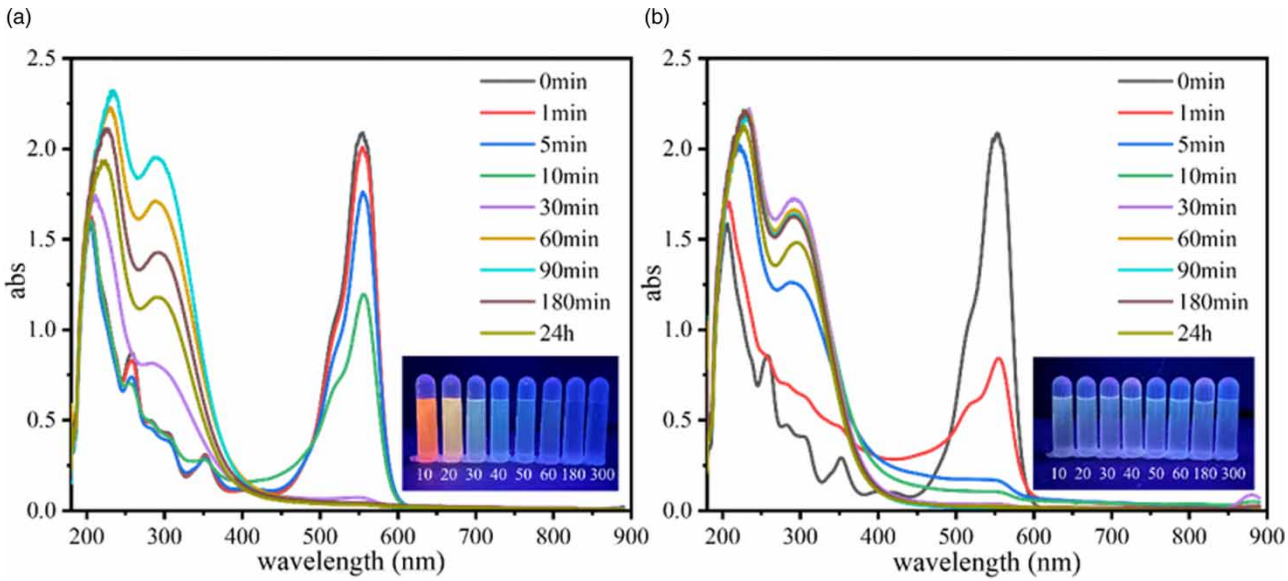

Figure 7 | UV-VIS absorption spectra of the reaction solution in the CF-nZVI-JE/PDS (a) and nZVI-JE/PDS (b) systems (The inset showed the colors of the solution at different time under 365 UV light).

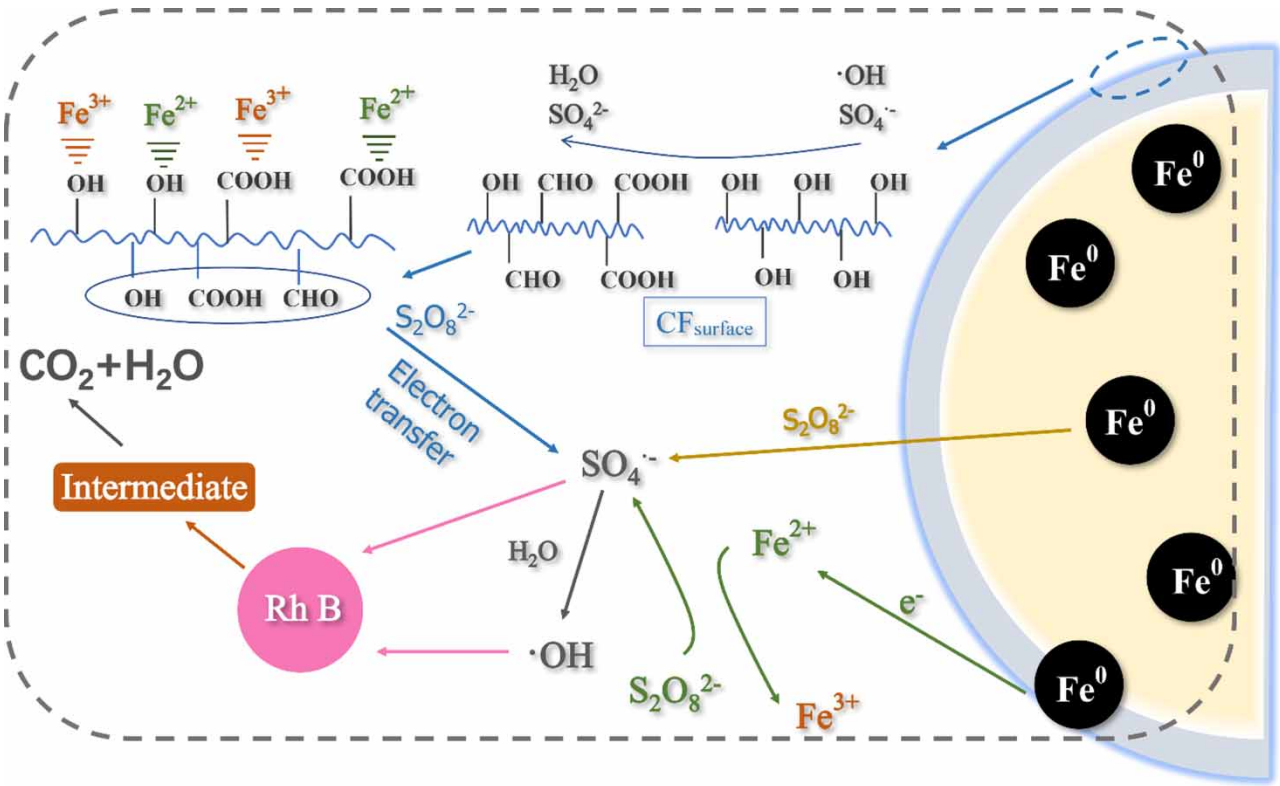

Figure 8 | Degradation mechanism of Rh B in the CF-nZVI-JE/PDS system.

60–100 nm and chain-type agglomeration of nanoparticles. The cellulose film wrapped outside the CF-nZVI-JE prevented the leakage of nZVI. The CF-nZVI-JE can efficiently activate PDS to degrade Rh B. Under the optimal activating conditions ($T = 25$ °C, [Rh B] = 50 mg/L, [$K_2S_2O_8$] = 1 g/L, JE = 0.5 g/L, pH = 4), the degradation rate of Rh B reached 99% within 30 min. The degradation process fit the pseudo-second-order kinetic model, indicating that the degradation process was involved in chemical adsorption. Compared with NO_3^- and SO_4^{2-}, the coexistence of Cl^- had a significant negative effect on Rh B degradation. Cycling experiment displayed that the degradation rate of Rh B still reached 86% after five cycles, suggesting that the CF-nZVI-JE had good reusability. Mechanism study demonstrated that the activation of PDS by the CF-nZVI-JE included three ways: (1) redox action of Fe^{2+}/Fe^{3+}; (2) nZVI mediated activation; (3) O-containing groups as an activator of the electron-transfer mediator. The degradation of Rh B in the CF-nZVI-JE/PDS system was involved in $SO_4^{\cdot-}$ and ·OH, and $SO_4^{\cdot-}$ was the main activation radical. The introduction of CF was conducive to the mineralization of Rh B. In addition, compared with the nZVI-JE, the CF-nZVI-JE obviously reduced the release amount of iron ions.

ACKNOWLEDGEMENTS

This work was financially supported by Science & Technology Program of Sichuan Province (2022YFS0503, 2021YFS0284).

DATA AVAILABILITY STATEMENT

All relevant data are included in the paper or its Supplementary Information.

CONFLICT OF INTEREST

The authors declare there is no conflict.

REFERENCES

Anipsitakis, G. P. & Dionysiou, D. D. 2004 Radical generation by the interaction of transition metals with common oxidants. *Environmental Science & Technology* **38**, 3705–3712.

Baldermann, A., Kaufhold, S., Dohrmann, R., Baldermann, C., Letofsky-Papst, I. & Dietzel, M. 2021 A novel nZVI–bentonite nanocomposite to remove trichloroethene (TCE) from solution. *Chemosphere* **282**, 131018.

Barzegar, G., Jorfi, S., Zarezade, V., Khatebasreh, M., Mehdipour, F. & Ghanbari, F. 2018 4-Chlorophenol degradation using ultrasound/peroxymonosulfate/nanoscale zero valent iron: reusability, identification of degradation intermediates and potential application for real wastewater. *Chemosphere* **201**, 370–379.

Chen, C., Liu, J. G., Gen, C., Liu, Q., Zhu, X. T., Qi, W. Z. & Wang, F. 2021 Synthesis of zero-valent iron/biochar by carbothermal reduction from wood waste and iron mud for removing Rhodamine B. *Environmental Science and Pollution Research* **28**, 48556–48568.

Chokejaroenrat, C., Sakulthaew, C., Satapanajaru, T., Tikhamram, T., Pho-Ong, A. & Mulseesuk, T. 2015 Treating methyl orange in a two-dimensional flow tank by in situ chemical oxidation using slow-release persulfate activated with zero-valent iron. *Environmental Engineering Science* **32**, 1007–1015.

Collivignarelli, M. C., Abba, A., Miino, M. C. & Damiani, S. 2019 Treatments for color removal from wastewater: state of the art. *Journal of Environmental Management* **236**, 727–745.

Dai, H. Y., Bao, J. G., Du, J. K. & Li, X. 2022 Efficiency and mechanism of photodegradation of rhodamine B by persulfate activated by MIL-101 (Fe, Cu). *Safety and Environmental Engineering* **29**, 223–231.

Dong, H. R., Zhao, F., Zeng, G. M., Tang, L., Fan, C. Z., Zhang, L. H., Zeng, Y. L., He, Q., Xie, Y. K. & Wu, Y. N. 2016 Aging study on carboxymethyl cellulose-coated zero-valent iron nanoparticles in water: chemical transformation and structural evolution. *Journal of Hazardous Materials* **312**, 234–242.

Dong, H. Y., Qiang, Z. M., Hu, J. & Sans, C. 2017 Accelerated degradation of iopamidol in iron activated persulfate systems: roles of complexing agents. *Chemical Engineering Journal* **316**, 288–295.

Eljamal, O., Eljamal, R., Maamoun, I., Khalil, A. M. E., Shubair, T., Falyouna, O. & Sugihara, Y. 2021 Efficient treatment of ammonia-nitrogen contaminated waters by nano zero-valent iron/zeolite composite. *Chemosphere* **287**, 131990.

Elmobarak, W. F., Hameed, B. H., Almomani, F. & Abdullah, A. Z. 2021 A review on the treatment of petroleum refinery wastewater using advanced oxidation processes. *Catalysts* **11**, 782.

Fu, F. L., Dionysiou, D. D. & Liu, H. 2014 The use of zero-valent iron for groundwater remediation and wastewater treatment: a review. *Journal of Hazardous Materials* **267**, 194–205.

Fu, X. Y., Zhao, W. T., Du, J. K., Zhou, Y. & Wei, L. Y. 2020 Degradation of Rhodamine B by nano-scale zero-valent iron activated persulfate. *China Water & Wastewater* **36**, 57–62.

Gao, Y. W., Zhang, Z. Y., Li, S. M., Liu, J., Yao, L. Y., Li, Y. X. & Zhang, H. 2016 Insights into the mechanism of heterogeneous activation of persulfate with a clay/iron-based catalyst under visible LED light irradiation. *Applied Catalysis B: Environmental* **185**, 22–30.

Gao, Y. J., Champagne, P., Blair, D., He, O. W. & Song, T. H. 2020 Activated persulfate by iron-based materials used for refractory organics degradation: a review. *Water Science and Technology* **81**, 853–875.

Guo, H. S., Su, S. N., Liu, Y., Ren, X. H. & Guo, W. L. 2020 Enhanced catalytic activity of MIL-101(Fe) with coordinatively unsaturated sites for activating persulfate to degrade organic pollutants. *Environmental Science and Pollution Research* **27**, 17194–17204.

Hameed, B. B. & Ismail, Z. Z. 2021 Biodegradation of reactive yellow dye using mixed cells immobilized in different biocarriers by sequential anaerobic/aerobic biotreatment: experimental and modelling study. *Environment Technology* **42**, 2991–3010.

He, F., Zhao, D. Y., Liu, J. C. & Roberts, C. B. 2007 Stabilization of Fe-Pd nanoparticles with sodium carboxymethyl cellulose for enhanced transport and dechlorination of trichloroethylene in soil and groundwater. *Industrial & Engineering Chemistry Research* **46**, 29–34.

Hou, M. F., Liao, L., Zhang, W. D., Tang, X. Y., Wan, H. F. & Yin, G. F. 2011 Degradation of rhodamine B by Fe(0)-based Fenton process with H_2O_2. *Chemosphere* **83**, 1279–1283.

Jiang, L. L., Zhang, Y., Zhou, M. H., Liang, L. & Li, K. R. 2018 Oxidation of Rhodamine B by persulfate activated with porous carbon aerogel through a non-radical mechanism. *Journal of Hazardous Materials* **358**, 53–61.

Khajouei, G., Finklea, H. O. O. & Lin, L. S. 2022 UV/chlorine advanced oxidation processes for degradation of contaminants in water and wastewater: a comprehensive review. *Journal of Environmental Chemical Engineering* **10**, 107508.

Kyzas, G. Z., Mengelizadeh, N., Saloot, M. K., Mohebi, S. & Balarak, D. 2022 Sonochemical degradation of ciprofloxacin by hydrogen peroxide and persulfate activated by ultrasound and ferrous ions. *Colloids and Surfaces A: Physicochemical and Engineering Aspects* **642**, 128627.

Lakkaboyana, S. K., Khantong, S., Asmel, N. K., Obaidullah, S., Kumar, V., Kannan, K., Venkateswarlu, K., Yuzir, A. & Yaacob, W. Z. W. 2021 Indonesian Kaolin supported nZVI (IK-nZVI) used for the efficient removal of Pb(II) from aqueous solutions: kinetics, thermodynamics and mechanism. *Journal of Environmental Chemical Engineering* **9**, 106483.

Lau, T. K., Chu, W. & Graham, N. J. D. 2007 The aqueous degradation of butylated hydroxyanisole by UV/$S_2O_8^{2-}$: study of reaction mechanisms via dimerization and mineralization. *Environmental Science & Technology* **41**, 613–619.

Ledakowicz, S. & Pazdzior, K. 2021 Recent achievements in dyes removal focused on advanced oxidation processes integrated with biological methods. *Molecules* **26** (4), 870.

Lee, J., von Gunten, U. & Kim, J. H. 2020 Persulfate-based advanced oxidation: critical assessment of opportunities and roadblocks. *Environmental Science & Technology* **54**, 3064–3081.

Li, S., Tang, J. C., Yu, C., Liu, Q. L. & Wang, L. 2022 Efficient degradation of anthracene in soil by carbon-coated nZVI activated persulfate. *Journal of Hazardous Materials* **431**, 128581.

Ma, D. S., Yi, H., Lai, C., Liu, X. G., Huo, X. Q., An, Z. W., Li, L., Fu, Y. K., Li, B. S. & Zhang, M. M., Lei, Q., Liu, S. Y. & Yang, L. 2021 Critical review of advanced oxidation processes in organic wastewater treatment. *Chemosphere* **275**, 130104.

Mateus, G. A. P., dos Santos, T. R. T., Sanches, I. S., Silva, M. F., de Andrade, M. B., Paludo, M. P., Gomes, R. G. & Bergamasco, R. 2020 Evaluation of a magnetic coagulant based on Fe_3O_4 nanoparticles and Moringa oleifera extract on tartrazine removal: coagulation-adsorption and kinetics studies. *Environment Technology* **41**, 1648–1663.

Matzek, L. W. & Carter, K. E. 2016 Activated persulfate for organic chemical degradation: a review. *Chemosphere* **151**, 178–188.

Nawaz, H., Umar, M., Ullah, A., Razzaq, H., Zia, K. M. & Liu, X. 2021 Polyvinylidene fluoride nanocomposite super hydrophilic membrane integrated with polyaniline-graphene oxide nano fillers for treatment of textile effluents. *Journal of Hazardous Materials* **403** (2021), 123587.

Pu, M. J., Ma, Y. W., Wan, J. Q., Wang, Y., Huang, M. Z. & Chen, Y. M. 2014 Fe/S doped granular activated carbon as a highly active heterogeneous persulfate catalyst toward the degradation of Orange G and diethyl phthalate. *Journal of Colloid & Interface Science* **418**, 330–337.

Qiong, B. 2020 *Study on Removal of Pollutants in Water by Sulfide-Modifed Nanoscale Zero-Valent Iron/Graphene Aerogel Composite. Thesis*.

Tan, Y., Zheng, S. L., Di, Y. H., Li, C., Bian, R. Z. & Sun, Z. M. 2021 Diatomite supported nano zero valent iron with 3D network for peroxymonosulfate activation in efficient degradation of bisphenol A. *Journal of Materials Science & Technology* **95**, 57–69.

Waldemer, R. H., Tratnyek, P. G., Johnson, R. L. & Nurmi, J. T. 2007 Oxidation of chlorinated ethenes by heat-activated persulfate: kinetics and products. *Environmental Science & Technology* **41**, 1010–1015.

Wang, X. Y., Ke, C. Q., Tang, C. P., Yuan, D. & Ye, Y. 2009 9,10-Dihydrophenanthrenes and Phenanthrenes from Juncus setchuensis. *Journal of Natural Products* **72**, 1209–1212.

Wang, G. L., Chen, S., Quan, X., Yu, H. T. & Zhang, Y. B. 2017 Enhanced activation of peroxymonosulfate by nitrogen doped porous carbon for effective removal of organic pollutants. *Carbon* **115**, 730–739.

Wang, X. Y., Du, Y., Liu, H. L. & Ma, J. 2018 Ascorbic acid/Fe-0 composites as an effective persulfate activator for improving the degradation of Rhodamine B. *RSC Advances* **8**, 12791–12798.

Wang, B., Deng, C. X., Ma, W. & Sun, Y. B. 2021 Modified nanoscale zero-valent iron in persulfate activation for organic pollution remediation: a review. *Environmental Science and Pollution Research* **28**, 34229–34247.

Wu, Y., Ou, P. F., Song, J., Zhang, L., Lin, Y. C., Song, P. F. & Xu, J. 2020 Synthesis of praseodymium-and molybdenum-sulfide nanoparticles for dye-photodegradation and near-infrared deep-tissue imaging. *Materials Research Express* **7**, 036203.

Xiao, S., Cheng, M., Zhong, H., Liu, Z. F., Liu, Y., Yang, X. & Liang, Q. H. 2020 Iron-mediated activation of persulfate and peroxymonosulfate in both homogeneous and heterogeneous ways: a review. *Chemical Engineering Journal* **384**, 123265.

Yan, J. C., Han, L., Gao, W. G., Xue, S. & Chen, M. F. 2015 Biochar supported nanoscale zerovalent iron composite used as persulfate activator for removing trichloroethylene. *Bioresource Technology* **175**, 269–274.

Yang, S. Y., Yang, X., Shao, X. T., Niu, R. & Wang, L. L. 2011 Activated carbon catalyzed persulfate oxidation of Azo dye acid orange 7 at ambient temperature. *Journal of Hazardous Materials* **186**, 659–666.

Yin, R. L., Guo, W. Q., Wang, H. Z., Du, J. S., Zhou, X. J., Wu, Q. L., Zheng, H. S., Chang, J. S. & Ren, N. Q. 2018 Enhanced peroxymonosulfate activation for sulfamethazine degradation by ultrasound irradiation: performances and mechanisms. *Chemical Engineering Journal* **335**, 145–153.

Zhang, H., Fu, H. & Zhang, D. B. 2009 Degradation of CI Acid Orange 7 by ultrasound enhanced heterogeneous Fenton-like process. *Journal of Hazardous Materials* **172**, 654–660.

Zhang, Y. Q., Zuo, S. J., Zhou, M. H., Liang, L. & Ren, G. B. 2018 Removal of tetracycline by coupling of flow-through electro-Fenton and in-situ regenerative active carbon felt adsorption. *Chemical Engineering Journal* **335**, 685–692.

Zhang, S., Lyu, H. H., Tang, J. C., Song, B. R., Zhen, M. N. & Liu, X. M. 2019 A novel biochar supported CMC stabilized nano zero-valent iron composite for hexavalent chromium removal from water. *Chemosphere* **217**, 686–694.

Zhang, S. L., Zhong, L. F., Wang, J., Tang, A. D. & Yang, H. M. 2021 Porous carbon-based $MgAlF_5{\cdot}1.5H_2O$ composites derived from carbon-coated clay presenting super high adsorption capacity for Congo Red. *Chemical Engineering Journal* **406**, 126784.

Zhang, S. L., Li, W., Li, M. L., Lin, T., Su, K., Chen, J. M. & Yang, H. W. 2022 Efficient removal and detoxification of Cr(VI) by PEI-modified Juncus effuses with a natural 3D network structure. *Separation and Purification Technology* **297**, 121543.

Zheng, H. L., Zhang, Z. M., Tang, M. F., Yi, Q., Chen, C. Y. & Peng, Z. C. 2006 The oxidation degradation of great green SF by Fenton reagent. *Spectroscopy and Spectral Analysis* **26**, 768–771.

Zhou, S. J., Xia, L. J., Zhang, K., Fu, Z., Wang, Y. L., Zhang, Q., Zhai, L. S., Mao, Y. S. & Xu, W. L. 2020 Titanium dioxide decorated natural cellulosic Juncus effusus fiber for highly efficient photodegradation towards dyes. *Carbohydrate Polymers* **232**, 115830.

First received 10 October 2022; accepted in revised form 21 December 2022. Available online 28 December 2022